

#### **OPEN ACCESS**

## SEI-Electrolyte Dyads for Dendrite Suppression in Li-Metal Batteries

To cite this article: Weiyu Li et al 2025 J. Electrochem. Soc. 172 070524

View the article online for updates and enhancements.

#### You may also like

- <u>Study on Gradation and Performance of Cold Patch Asphalt Mixtures</u>
  Li Qiang, Liu Feiyi, Luo Xiao et al.
- (Invited) Lithium-Ion Endohedral Fullerenes on Carbon Nanotube Electrode-Laminated Perovskite Solar Cells As Dopants and Anti-Oxidants II Jeon, Ahmed Shawky, Esko Kauppinen et al.
- <u>Understanding Temperature Stability of Surface Cation Dopants on LSCF Electrodes</u>
  Sophie Coppieters 't Wallant, Filip Grajkowski, Bill Liu et al.

# **ECC-Opto-10 Optical Battery Test Cell: Visualize the Processes Inside Your Battery!**



- Battery Test Cell for Optical Characterization Designed for light microscopy, Raman spectroscopy and XRD.
- ✓ Optimized, Low Profile Cell Design (Device Height 21.5 mm) Low cell height for high compatibility, fits on standard samples stages.
- ✓ High Cycling Stability and Easy Handling
  Dedicated sample holders for different electrode arrangements included!
- Cell Lids with Different Openings and Window Materials Available





#### Contact us:

- +49 40 79012-734
- sales@el-cell.com
- www.el-cell.com









### SEI-Electrolyte Dyads for Dendrite Suppression in Li-Metal Batteries

Weiyu Li, 1,2 William Korbitz, Hamdi A. Tchelepi, and Arnaud Tran Tran

The solid-electrolyte interphase (SEI) plays a crucial role in Li-metal batteries, yet its influence on dendritic growth remains poorly understood. We present a physics-based stability analysis of dendrite initiation explicitly incorporating a SEI layer between the Limetal anode and electrolyte, without assuming electroneutrality. Our model examines how SEI transport properties, thickness, and interfacial energy interact with electrolyte characteristics (diffusion coefficient, permittivity, interfacial energy) and operating conditions to govern interfacial morphological stability. We derive closed-form expressions linking dendrite growth rate to measurable parameters and construct analytical phase diagrams identifying regimes of stability and instability under both underlimiting and overlimiting conditions. Relaxing the electroneutrality assumption enables the model to capture space-charge effects essential for understanding dendrite behavior at high current densities. The analysis reveals that the SEI can either suppress or promote dendrite growth depending on its interaction with the electrolyte. Interfacial stability is enhanced by a high SEI ionic conductivity-to-electrolyte diffusivity ratio and a high Li-SEI to Li-electrolyte interfacial energy ratio. These findings show that stability is governed not by SEI properties alone, but by SEI-electrolyte coupled property dyads that define the phase space. This framework enables predictive interfacial design and offers a roadmap for tailoring artificial SEI to specific electrolytes. © 2025 The Author(s). Published on behalf of The Electrochemical Society by IOP Publishing Limited. This is an open access article distributed under the terms of the Creative Commons Attribution 4.0 License (CC BY, https://creativecommons.org/ licenses/by/4.0/), which permits unrestricted reuse of the work in any medium, provided the original work is properly cited. [DOI: 10.1149/1945-7111/adf013]

Manuscript submitted May 29, 2025; revised manuscript received June 20, 2025. Published July 24, 2025.

Dendritic lithium (Li) growth remains one of the most critical challenges limiting the safety and longevity of Li-metal batteries. Dendrites form during charging when Li deposition at the anode becomes non-uniform and grow to needle-like metallic Li protrusions. This interfacial instability typically arises from a transition from reaction-limited to transport-limited deposition kinetics, especially under high current conditions. 1,2 Factors influencing this instability include the ionic transport properties in the electrolyte, mechanical stress in the electrode-electrolyte interface, 4 the microscale roughness of the Li surface,<sup>5</sup> and the interfacial chemistry and structure of the solid-electrolyte interphase (SEI).<sup>6</sup> Once formed, dendrites can penetrate the separator and cause internal short circuits or become electrically disconnected, resulting in inactive "dead Li" and capacity loss.<sup>2,7</sup> Understanding and controlling dendrite initiation is critical for the safe and efficient operation of high energy density Li-metal batteries.

SEI is a nanoscale interphase formed on the anode surface from electrolyte decomposition and metal-electrolyte reactions during initial charging cycles. It typically exhibits a heterogeneous, multilayered structure that comprises inorganic compounds near the electrode and organic species closer to the electrolyte.8-10 Although thin (typically 10–100 nm), 11 the SEI plays an important role in mediating Li-ion transport and electrochemical reactions. Artificial SEI layers have been proposed to enhance anode protection by replicating or improving the natural SEI.<sup>12</sup> Conventionally, an ideal SEI is expected to exhibit high Li-ion conductivity, low electronic conductivity, and robust mechanical and thermal stability to enable fast ion transport and prevent cracking and continuous electrolyte consumption. 13 Yet, its dynamic formation and evolution under battery operation remain elusive, and neglecting it in theoretical models can obscure key mechanisms behind dendrite initiation and propagation.<sup>2,14</sup>

The experimental study of SEI's role in dendrite suppression is challenging due to its thinness and chemical complexity. Advanced in situ and ex situ techniques, including cryo-TEM, SEM, and AFM, have revealed both protective and destabilizing roles of the SEI, depending on its composition, nanostructure and morphology, and

the resulting physical and electrochemical properties. SEIs with high ionic conductivity have been shown to reduce dendrite formation, but a quantitative description between ionic conductivity and dendrite suppression remains unclear. 15,16 Interfacial energy also plays an important role, materials with higher surface energy tend to suppress dendrite growth by stabilizing the electrode interface. Cryo-TEM studies indicate that cracking and localized mechanical failure of the SEI exposes fresh Li, which acts as new nucleation sites for dendrites. 18 Conflicting results have emerged regarding mechanical modulus: high-modulus SEIs are theoretically predicted to suppress dendrites, yet low-modulus, flexible organic-rich SEIs have been observed to enable uniform Li deposition. 4,19,20 This contradiction suggests that mechanical properties alone are insufficient and must be complemented by a coupled physico-electrochemical understanding. Additionally, uniform SEI thickness has been identified to avoid localized current hot spots, though few studies have quantified this factor experimentally. <sup>21</sup> These findings underline both the promise and the uncertainty in designing SEIs to prevent dendrite initiation effectively. A systematic framework is needed to describe and quantify how SEI properties, i.e., ionic conductivity, interfacial energy, mechanical modulus, and thickness, collectively influence dendrite growth under varying operating

Given the experimental challenges, computational modeling provides a promising pathway to uncover the fundamental mechanisms of dendrite growth and SEI influence. However, most existing models simplify or omit the SEI due to its thinness relative to the bulk electrode and electrolyte. Classical porous electrode models, i.e., pseudo-2-dimensional models often treat the SEI as a lumped resistance term or ignore it entirely, <sup>22–25</sup> with few efforts accounting for mass, charge and thermal transport within the SEI based on its specific physicochemical properties. 26–29 Pore-scale methods such as phase-field modeling and smooth particle hydrodynamics have incorporated SEI effects by modifying reaction kinetics, offering valuable insights into interfacial dynamics. More recent studies, including kinetic Monte Carlo simulations<sup>32</sup> and linear stability analyses<sup>33</sup> treat the SEI more explicitly. These models often adopt the electroneutrality assumption to simplify electrolyte behavior; however, this assumption breaks down near the electrode under high current densities.<sup>3</sup> Thus, modeling approaches that capture both the

<sup>&</sup>lt;sup>1</sup>Department of Mechanical Engineering, University of Wisconsin-Madison, Madison, Wisconsin 53706, United States of America

<sup>&</sup>lt;sup>2</sup>Department of Energy Science and Engineering, Stanford University, Stanford, California 94305, United States of America <sup>3</sup>VoltaBack Inc., Levallois-Perret 92300, France

nanoscale physics of the SEI and the non-electroneutral behavior of the electrolyte remain rare but necessary for a predictive understanding of dendrite initiation. Emerging studies on dendrite suppression using interfacial buffer layers between Li-metal and solid electrolytes suggest that dendrite suppression depends not solely on SEI properties but on the coupled behavior of the SEI-electrolyte system.<sup>34</sup> This coupling may help explain inconsistent findings in the literature regarding SEI modulus and interfacial stability. Specifically, stabilization and destabilization effects must be interpreted based on SEI-electrolyte dyads, which reflect coupled physico-electrochemical-mechanical interactions.

In this work, we present a physics-based linear stability analysis of dendrite initiation that explicitly incorporates a SEI layer between the Li-metal anode and the electrolyte, without assuming electroneutrality. We examine how SEI transport properties (e.g., ionic conductivity), thickness, and interfacial energy at the Li-SEI interface interact with electrolyte properties (e.g., diffusion coefficient, permittivity, and Li-electrolyte interfacial energy) and operating conditions to influence interfacial stability. Our analytical model reveals that the SEI can either stabilize or destabilize the interface, depending on the SEI-electrolyte dyad's coupled properties. We derive closed-form expressions linking dendrite growth rate to measurable parameters and construct analytical phase diagrams that map regimes of stability and instability based on key nondimensional ratios, such as the ionic conductivity-to-diffusion coefficient ratio and the interfacial energy ratio. These diagrams identify conditions under which the SEI enhances interfacial stability and suppresses dendrite growth compared to the absence of an SEI layer. We demonstrate that interfacial stability is not governed by SEI properties alone, but by their dyadic interaction with the electrolyte environment. This framework provides design principles for SEI engineering by identifying optimal combinations of SEI and electrolyte properties. As such, effective SEI design must be tailored to the specific electrolyte system.

#### **Mathematical Formulation**

**Problem description.**—We study Li deposition on a Li-metal anode in a two-dimensional half-cell domain that includes a SEI layer,  $\Omega = \Omega_{\rm an} \cup \Omega_{\rm SEI} \cup \Omega_{\rm el}$ . As shown in Fig. 1, the domain consists of three regions: the Li-metal anode  $\Omega_{\rm an}$ , the SEI layer  $\Omega_{\rm SEI}$ , and the liquid electrolyte  $\Omega_{\rm el}$ . Initially (at time t=0), the interface  $\Gamma_{\rm in}(t)$  between the Li-metal anode and the SEI layer is flat, coinciding with the plane x=0, i.e.,  $\Gamma_{\rm in}(0)={\bf x}=(x,y)^{\rm T}$ : x=0, 0< y< B. A negative electrostatic potential  $\phi_{\rm e}$  is applied to the electrode surface  $\Gamma_{\rm in}(t)$  at all times, while the potential at the outer edge of the electrolyte (x=L) is maintained at 0.

The SEI/electrolyte interface  $\Gamma_{out}$ , separating  $\Omega_{SEI}$  from the liquid electrolyte  $\Omega_{el}$ , remains flat at all times. We relax the assumption of electroneutrality in the electrolyte and neglect fluid convection due to the thinness of the cell, treating the electrolyte as immobile. The initial concentration of lithium cations,  $\mathrm{Li}^+$ , in the electrolyte is  $c_0$ .

We model the SEI as an electronic insulator and an ionic conductor, with a constant Li<sup>+</sup> concentration  $c_+^{6,34}$  The SEI layer is considered pre-formed with a fixed thickness  $L_1$ , and no Faradaic reactions occur at the SEI/electrolyte interface  $\Gamma_{\rm out}$ . The SEI is assumed inert to anions. At the Li-metal/SEI interface  $\Gamma_{\rm in}(t)$ , Li cations (Li<sup>+</sup>) undergo Faradaic reactions with electrons ( $e^-$ ), reducing to Li atoms, i.e., Li<sup>+</sup> +  $e^ \rightarrow$  Li. The deposited Li increases the thickness of the anode  $h^{(0)}(t)$ .

Our objective is to identify the conditions and system parameters that lead to dendrite initiation during electrodeposition, with a key focus on determining the SEI/electrolyte dyad properties that can mitigate dendrite formation. We specifically examine how transport phenomena within the SEI layer influence the stability of the deposition process, as characterized by the temporal evolution of h(y, t). Mechanical phenomena such as SEI fracture, elastic deformation, or growth dynamics are beyond the scope of this model.

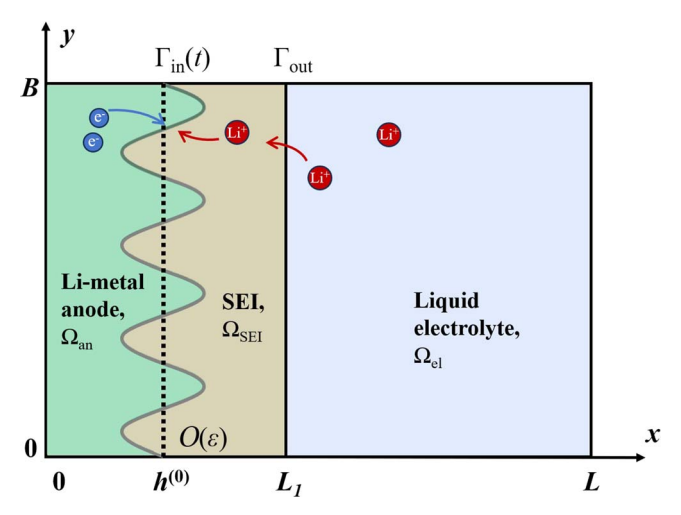


Figure 1. Schematic representation of a two-dimensional half-cell domain  $\Omega = \Omega_{\rm an} \cup \Omega_{\rm SEI} \cup \Omega_{\rm el}$ . The SEI layer  $\Omega_{\rm SEI}$  separates the Li-metal anode  $\Omega_{\rm an}$  from the liquid electrolyte,  $\Omega_{\rm el}$ . The anode surface,  $\Gamma_{\rm in}(t)$ , evolves over time due to electrodeposition, while the interface  $\Gamma_{\rm out}$  between the SEI layer and the electrolyte remains fixed.

However, interfacial energy effects are included through capillarity terms that penalize the creation of new surface area.

**Governing equations.**—Liquid electrolyte.—Under isothermal conditions and in the absence of a magnetic field, we define the mass flux of cations and anions at any point  $\mathbf{x} = (x, y)^{\mathsf{T}} \in \Omega_{\mathsf{el}} = \{\mathbf{x}: L_1 < x < L, 0 < y < B\}$  in the liquid electrolyte,

$$\mathbf{J}_{\pm} = -D_{\pm} \left( \nabla c_{\pm} + \frac{z_{\pm} c_{\pm} F}{RT} \nabla \phi_{\mathrm{el}} \right), \tag{1}$$

where  $c_{\pm}$  are the concentrations (molm<sup>-3</sup>) of the cations and anions;  $\phi_{\rm el}$  is the electric potential (V);  $D_{\pm}$  and  $z_{\pm}$  are the diffusion coefficients (m<sup>2</sup>s<sup>-1</sup>) and charge numbers (-) of the cations and anions; F is the Faraday constant (s·A/mol), R is the gas constant (J/mol/K), and T is the temperature (K). The Nernst-Planck Eqs. describe the mass conservation in the electrolyte.

$$\frac{\partial c_{\pm}}{\partial t} = -\nabla \cdot \mathbf{J}_{\pm}, \quad \mathbf{x} \in \Omega_{\text{el}}.$$
 [2]

We relax the assumption of electroneutrality  $(z_+c_+ + z_-c_- = 0)$  in the liquid electrolyte, where the electric potential,  $\phi_{\rm el}$ , is governed by the Poisson equation,

$$-\epsilon \nabla^2 \phi_{\rm el} = F(z_+ c_+ + z_- c_-), \quad \mathbf{x} \in \Omega_{\rm el},$$
 [3]

where  $\epsilon$  is the absolute permittivity of the solvent (F m<sup>-1</sup>).

Solid-electrolyte interphase (SEI).—The SEI is modeled as an electronic insulator and Li<sup>+</sup> conductor. <sup>6,34</sup> The Faradaic reactions of Li<sup>+</sup> occur exclusively on the anode surface, not at the interface between the electrolyte and the SEI. The spatial distribution of the electric potential,  $\phi_{\rm SEI}({\bf x},t)$ , within the SEI is governed by the Laplace equation,

$$\nabla \cdot \mathbf{i}_{\text{SEI}} = 0, \quad \mathbf{i}_{\text{SEI}} = -\sigma_{\text{SEI}} \nabla \phi_{\text{SFI}}, \quad \mathbf{x} \in \Omega_{\text{SEI}},$$
 [4]

where  $\sigma_{\rm SEI}$  and  $\mathbf{i}_{\rm SEI}$  are the ionic conductivity (S m<sup>-1</sup>) of Li<sup>+</sup> and the current density (A/m<sup>2</sup>) in the SEI. At the Li-metal surface, the normal component of  $\mathbf{i}_{\rm SEI}$  is related to the applied current density I,

$$\mathbf{n} \cdot \mathbf{i}_{SEI} = I, \quad \mathbf{x} \in \Gamma_{in}.$$
 [5]

The interfacial current density I is given by the Butler-Volmer kinetic,

$$I = -\frac{zFk_0}{\gamma_{ts}} \left[ \exp\left(\alpha_{an} \frac{zF\eta_{\alpha} + 2\omega\gamma_{Li}^{SEI} \kappa}{RT}\right) - \frac{c_{+}(\mathbf{x} \in \Gamma_{in}, t)}{c^{\Theta}} \exp\left(-\alpha_{cat} \frac{zF\eta_{\alpha} + 2\omega\gamma_{Li}^{SEI} \kappa}{RT}\right) \right],$$
 [6]

where  $k_0$  is the reaction rate constant (mol·m² s<sup>-1</sup>),  $\gamma_{\rm ts}$  is the activity coefficient of the transition state for the Faradaic reaction (-), z is the number of electrons involved in the electrode reaction,  $\alpha_{\rm an}$  and  $\alpha_{\rm cat}$  are the anodic and cathodic charge-transfer coefficients (-), we set  $\alpha_{\rm an} = \alpha_{\rm cat} = 0.5$ ,  $c^{\Theta}$  is the standard concentration,  $\omega$  is the molar volume of Li-metal (m³ mol<sup>-1</sup>),  $\gamma_{\rm Li}^{\rm SEI}$  is the isotropic interfacial energy of the Li-metal with the SEI (J m<sup>-2</sup>), and  $\kappa$  is the mean curvature of the electrode's surface (m<sup>-1</sup>). The activation overpotential  $\eta_{\Omega}(\mathbf{x} \in \Gamma_{\rm in}, t)$  is defined as,

$$\eta_{\alpha} = \phi_{e} - \phi_{SEI}(\mathbf{x} \in \Gamma_{in}, t) - E^{\Theta}$$
[7]

where  $E^{\Theta}$  is the standard electrode potential. We set  $\gamma_{\rm ts}=1$  and  $E^{\Theta}=0$ .

At  $x = L_1$ , the interface between the SEI and the liquid electrolyte is inert to anions, i.e., the normal component of the mass flux of anions,  $\mathbf{J}_{-} = (J_{-x}, J_{-y})^{\mathsf{T}}$ , is 0,

$$J_{-x}(L_1, y, t) = 0.$$
 [8]

The normal component of the current density in the SEI,  $\mathbf{i}_{\text{SEI}} = (i_{\text{SEI},x}, i_{\text{SEI},y})^{\mathsf{T}}$ , at  $x = L_1$  is proportional to the normal component of the mass flux of cations,  $\mathbf{J}_+ = (J_{+,x}, J_{+,y})^{\mathsf{T}}$ , entering the SEI from the electrolyte,

$$i_{SEI,r}(L_1, y, t) = zFJ_{+,r}(L_1, y, t),$$
 [9]

which ensures mass conservation of cations across the SEI/electrolyte interface. In addition to 8 and 9, we also enforce a minimum Li<sup>+</sup> concentration condition at the SEI/electrolyte interface,<sup>3</sup>

$$\frac{\partial c_+}{\partial x}(L_1, y, t) = 0.$$
 [10]

At the interface between the SEI and the electrolyte, we enforce continuity of the electric potential and the normal components of the current density,

$$\phi_{SEI}(L_1, y, t) = \phi_{el}(L_1, y, t),$$

$$i_{SEI,x}(L_1, y, t) = i_{el,x}(L_1, y, t),$$
[11]

The rate of change of Li-metal surface height h(y, t) is given by the current density into the anode,

$$\mathbf{e}_{\mathbf{x}} \cdot \mathbf{n} \frac{\partial h}{\partial t} = -\frac{\omega I}{zF}.$$
 [12]

The curvature and the normal vector are related to the surface function h(y, t),  $^{35}$ 

$$\mathbf{n} = \frac{1}{\sqrt{1 + (\partial_y h)^2}} \begin{pmatrix} -1\\ \partial_y h \end{pmatrix}, \quad \kappa = -\frac{1}{2} \frac{\partial_y^2 h}{[1 + (\partial_y h)^2]^{3/2}}.$$
 [13]

The boundary conditions on the remaining segments of the computational domain are

$$\phi_{el} = 0, \quad c_{+} = c_{0}, \quad c_{-} = c_{0}, \quad \text{for } x = L;$$
 [14a]

$$\frac{\partial \phi_{\text{el}}}{\partial y} = 0$$
,  $\frac{\partial c_{+}}{\partial y} = 0$ ,  $\frac{\partial c_{-}}{\partial y} = 0$ , for  $y = 0$  and  $B$ . [14b]

#### Linear Stability Analysis

The linear stability analysis introduces a small perturbation  $\varepsilon \exp(wt + iky)$  to a one-dimensional steady-state base state. This base state is defined by a flat electrode surface  $h^{(0)}(t) \equiv Ut$  moving at constant velocity  $U = dh/dt = \omega I^{(0)}/(zF)$ , along with corresponding profiles for electric potential  $\phi^{(0)}(x)$ , cation concentration  $c_+^{(0)}(x)$ , and anion concentration  $c_-^{(0)}(x)$ . The goal is to derive a dispersion relation that links the perturbation growth rate w (s<sup>-1</sup>) to its wavenumber k (m<sup>-1</sup>). The perturbation on the surface of the electrode and the state variables are

$$h = h^{(0)}(t) + \hat{\varepsilon}h^{(1)}, \quad \phi = \phi^{(0)}(x) + \hat{\varepsilon}\phi^{(1)},$$

$$c_{+} = c_{+}^{(0)}(x) + \hat{\varepsilon}c_{+}^{(1)}, \quad \hat{\varepsilon} = \varepsilon e^{wt + iky},$$
[15]

where the constant  $h^{(1)}$  and the functions  $\phi^{(1)}(x)$  and  $c_{\pm}^{(1)}(x)$  are first-order (in  $\varepsilon$ ) corrections to the base state denoted by the superscript  $^{(0)}$ .

If the perturbation increases with time, indicating a positive growth rate (w > 0), the electrodeposition process is considered unstable and susceptible to dendrite initiation. If the perturbation has a negative growth rate for all wavelengths, any dendrite initiation, equivalent to a small perturbation at the electrode surface, would decay over time, and the electrodeposition process is considered stable and flat.

It follows from Eq. 13 that first-order approximations of its unit normal vector,  $\mathbf{n} = \mathbf{n}^{(0)} + \mathcal{O}(\varepsilon^2)$ , and curvature,  $\kappa = \kappa^{(0)} + \hat{\varepsilon}\kappa^{(1)}$ , are given by

$$\mathbf{n}^{(0)} = \begin{pmatrix} -1\\ 0 \end{pmatrix}, \quad \kappa^{(0)} = 0, \quad \kappa^{(1)} = \frac{k^2}{2}h^{(1)}.$$
 [16]

Derivations for the base-state and the perturbed-state Eqs. are displayed in Appendix A. We solve the resulting boundary-value problems (BVPs) for the base state (of order  $\varepsilon^0$ ) and the first-order correction (of order  $\varepsilon$ ). The results are reported below in terms of dimensionless growth rate, wavenumber, and current density,

$$\tilde{w} = \frac{wF^2c_0L^2}{\sigma_{\text{SEI}}RT}, \quad \tilde{k} = kL, \quad \text{and} \quad \tilde{I} = \frac{ILF}{RT\sigma_{\text{SEI}}}.$$
 [17]

#### **Results and Discussion**

The parameters used in our simulations are presented in Table I. We first perform numerical simulations to compute the base-state solutions under varying applied electric potentials,  $\phi_e$ , to establish the steady-state profiles of ionic species concentrations and the electric potential distribution across the SEI and electrolyte domains. Figure 2 shows the dimensionless concentrations of cations,  $\tilde{c}_{+}^{(0)}$ , and anions,  $\tilde{c}_{-}^{(0)}$ ; charge density  $\tilde{\rho}_{e}^{(0)} = \tilde{c}_{+}^{(0)} - \tilde{c}_{-}^{(0)}$ ; and electric potential  $\tilde{\phi}^{(0)}$ . The SEI layer occupies the region  $0 \leq \tilde{\xi} \leq 0.04$ . For small values of the applied potential,  $\phi_e = -0.1 \text{ V}$ , the cations at the SEI/ electrolyte interface are not depleted, and electroneutrality holds in the liquid electrolyte domain. Within the SEI,  $\tilde{c}_{+}^{(0)}$  remains constant while  $\tilde{c}_{-}^{(0)} = 0$  as the SEI is a Li<sup>+</sup> conductor and is impermeable to anions. At larger values of  $\phi_e$ , the  $\mathrm{Li}^+$  concentration  $\tilde{c}_+^{(0)}(\xi)$  becomes nearly zero near the electrode surface, and local electroneutrality is violated within the electrolyte boundary layer (0.04  $\leq \tilde{\xi} \leq$  0.2). As a result, the charge density  $\tilde{\rho}_{\rm e}^{(0)}$  in the SEI is higher under small applied potentials than under large ones, since cation depletion

Half-cell length Cation diffusivity Anion diffusivity Femperature Molecular weight of lithium metal Density of Li-metal Li+ bulk concentration	$egin{array}{c} L & & & & & & & & & & & & & & & & & & $	$0.5$ $1.61 \cdot 10^{-11}$ $3.91 \cdot 10^{-11}$ $298.15$	$\mu { m m} \ { m m}^2  { m s}^{-1} \ { m m}^2  { m s}^{-1}$	Ref. 3 Ref. 36
Cation diffusivity  Anion diffusivity  Femperature  Molecular weight of lithium metal  Density of Li-metal  Li <sup>+</sup> bulk concentration	$D_+ \ D \ T \ M$	$   \begin{array}{r}     1.61 \cdot 10^{-11} \\     3.91 \cdot 10^{-11} \\     298.15   \end{array} $	$\frac{m^2}{m^2} \frac{s^{-1}}{s^{-1}}$	Ref 36
Temperature  Molecular weight of lithium metal  Density of Li-metal  Li <sup>+</sup> bulk concentration	$egin{array}{c} D \ T \ M \end{array}$	298.15	$m^2 s^{-1}$	ICI. JU
Temperature  Molecular weight of lithium metal  Density of Li-metal  Li <sup>+</sup> bulk concentration	T M	298.15		Ref. 36
Molecular weight of lithium metal Density of Li-metal Li <sup>+</sup> bulk concentration		6.041	K	Ref. 3
Density of Li-metal Li <sup>+</sup> bulk concentration	0	6.941	g/mol	Ref. 37
Li <sup>+</sup> bulk concentration		0.534	g/cm <sup>3</sup>	Ref. 37
		1000	mol m <sup>3</sup>	Ref. 3
tandard concentration	$\overset{c_0}{c^\Theta}$	1000	mol m <sup>3</sup>	Ref. 3
tandard electrode potential	$E^{\Theta}$	0	V	
Dielectric constant	$\epsilon/\epsilon_0$	90	<u>.</u>	Ref. 38
acuum permittivity	$\epsilon_0$	$8.854 \cdot 10^{-12}$	${ m Fm}^{-1}$	Ref. 39
Reaction rate constant	$k_0$	$2.7 \cdot 10^{-3}$	$mol/m^2 s^{-1}$	Ref. 40
urface energy of metal/electrolyte interface	$\gamma$	1	J m <sup>2</sup>	Ref. 41
ctivity coefficient of the transition state	$\gamma_{ m ts}$	1	<del></del>	101. 11
deference ionic conductivity of the SEI		$1 \cdot 10^{-3}$	$\mathrm{S}\mathrm{m}^{-1}$	Ref. 13
EI thickness	$\sigma_{ m ref}$	20	nm	Ref. 6
EI IIICKIIESS	$L_1$	20	IIII	Kei. 0
1	'	1		
	//	©   0		
0.8	-	Anion concentration, $\tilde{c}_{-0.8}^{(0)}$		/ /
g   i		g   j		,
		.ig   <b>!</b>		
로 0.6		† 0.6 g		
ti   i		fa   !		
Cartion concentration, $c_{\rm c}^{(2)}$ 0.8 - $c_{\rm c}^{(2)}$ 0.8 - $c_{\rm c}^{(2)}$ 0.9		E I	/ /	
5 0.4	- 1	ŭ 0.4 -		
$\delta$   $-\phi_{e}$	= -0.1 V	8	$ \phi_{\rm o}$	= -0.1 V = -2 V
	= -2 V	g   i		2 V
i n 2	- <i>2</i> v	·H 0.2	γe	
S 0.2		4 0.2 I		
0 0.2 0.4 0.6	0.0 1	0	0.4 0.6	0.0 1
	0.8	0 0.2		0.8
Normalized distance, $\xi$		No	ormalized distance,	ξ
$\begin{array}{c} 0.25 \\                                    $	'	0		
		-10 - 1		
	= -0.1  V		<del></del>	$\phi_{\rm e} = -0.1 \; { m V} \;   \;$
<u>-</u> - φ <sub>e</sub>	= -0.1  V - = -2  V -	-20		$\phi_{\mathrm{e}} = -0.1 \mathrm{\ V}$ $\phi_{\mathrm{e}} = -2 \mathrm{\ V}$
i Pe		-f <sup>-20</sup> [   /	,	- ' -
0.15		tia li		
© 0.15 ×10 <sup>-3</sup>	1	± -30 - 1 · 1		
8 710	,	)   j		
6	11	o <sub>4</sub> -40 - 1		]
<u>z</u> 0.1	<b>'</b>	.01		
	1	£ 50   1.		
2		Electric potential, $\tilde{\phi}^{(0)}$		1
0.05	0.15	점   <b>!</b> /		
0.05 0.1	0.15			-
		}		
		-70		
0 0.2 0.4 0.6	0.8 1	0 0.2	0.4 0.6	0.8 1
Normalized distance, $\xi$			ormalized distance,	

Figure 2. Spatial profiles of the base-state cation,  $\tilde{c}_{+}^{(0)}$ , and anion,  $\tilde{c}_{-}^{(0)}$ , concentrations; charge density  $\tilde{\rho}_{e}^{(0)} = \tilde{c}_{+}^{(0)} - \tilde{c}_{-}^{(0)}$ ; and electric potential  $\tilde{\phi}^{(0)}$  for SEI ionic conductivity  $\sigma_{\text{SEI}} = 10^{-3} \text{ S m}^{-1}$  and at applied electric potentials  $\phi_{e} = -0.1 \text{ V}$  and -2 V.

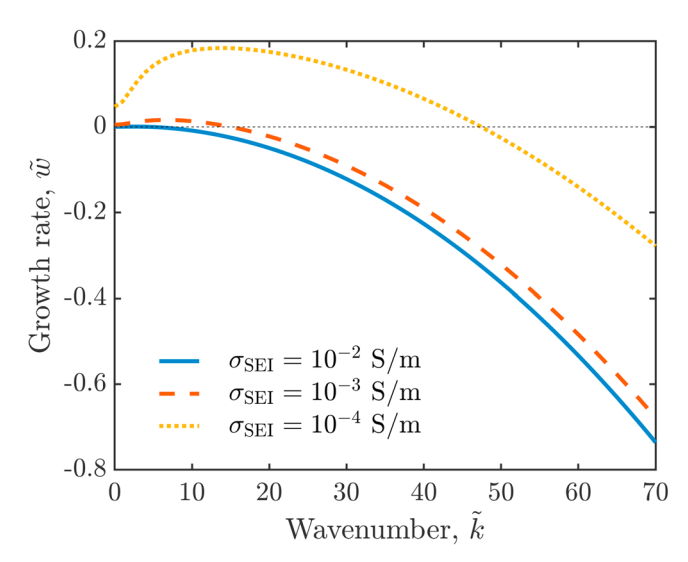


**Figure 3.** Dispersion relations  $\tilde{w} = \tilde{w}(\tilde{k})$  with different SEI layer ionic conductivities  $\sigma_{\rm SEI} = 10^{-2}, \, 10^{-3}$  and  $10^{-4}$  S m<sup>-1</sup> and at applied electric potential  $\phi_{\rm e} = -2$  V.

occurs near the SEI/electrolyte interface at higher potentials. As shown in Fig. 2, increasing  $\phi_e$  leads to a steeper electric potential gradient,  $\partial_{\xi}\tilde{\phi}^{(0)}$ , near the SEI/electrolyte interface. These trends are consistent with previously reported base-state profiles in the absence of an SEI layer.<sup>3</sup> Additionally, the electric potential  $\tilde{\phi}^{(0)}$  exhibits a linear drop across the SEI, from the SEI/electrolyte interface to the Li/SEI interface. The slope of this drop,  $\tilde{I}^{(0)}/\tilde{\sigma}_{\rm SEI}$ , increases with the magnitude of the applied current density (applied electric potential).

Figure 3 shows the dispersion relations,  $\tilde{w} = \tilde{w}(\tilde{k})$ , where the non-dimensional growth rate  $\tilde{w}$  is plotted against the wavenumber  $\tilde{k}$ for various SEI ionic conductivities. As  $\tilde{k}$  increases, the growth rate initially rises, reaching a peak at the maximum growth rate  $\tilde{w}_{max}$ , and then declines. Beyond a critical wavenumber  $\tilde{k}_{\rm cri}$ , the growth rate becomes negative, indicating the onset of morphological stability, i.e., Li deposition becomes stable and dendrite formation is suppressed. This stabilization arises from the surface energy penalty on the creation of additional surface area. This penalty is quantified by the term proportional to capillary number that corresponds to the interfacial energy between the Li-metal and SEI, Casel, or between the Li-metal and electrolyte in the absence of SEI,  $Ca_{Li}^{el}$ , in Eqs. 18 and 20. Wavenumber  $\tilde{k}$  is related to the nondimensional surface roughness wavelength  $\tilde{\lambda} = \lambda/L$  by  $\tilde{\lambda} = 2\pi/\tilde{k}$ .<sup>34</sup> Thus, using Li-metal anodes with surface roughness wavelengths smaller than the critical wavelength can help mitigate dendritic growth. Increasing the SEI ionic conductivity leads to a lower maximum growth rate  $\tilde{w}_{\text{max}}$  and a smaller critical wavenumber  $\tilde{k}_{\text{cri}}$ . This implies that a more ionic conductive SEI layer expands the range of stable modes and effectively suppresses dendrite growth. This trend aligns well with experimental findings, which have reported enhanced stability with more ionic conductive SEI materials. 13 Moreover, we find that the critical wavenumber scales inversely with the square root of the SEI ionic conductivity, i.e.,  $\tilde{k}_{\rm cri} \propto \sqrt{1/\tilde{\sigma}_{\rm SEI}}$ . This scaling relationship is also derived analytically and discussed in detail in Appendix B. Physically, this relationship highlights how improved ionic transport in the SEI reduces the electric field gradient and charge accumulation at sharp interface perturbations, thereby stabilizing the deposition front.<sup>3</sup>

We next derive analytical expressions for the dispersion relations under both underlimiting and overlimiting current conditions. Detailed derivations are provided in Appendix B. The resulting

relations  $\tilde{w} = \tilde{w}(\tilde{k})$ , describe the growth rate  $\tilde{w}$  of perturbations as a function of non-dimensional wavenumber  $\tilde{k}$  and system parameters. Under low and high current regimes, the dispersion relations in the presence of a SEI layer are:

$$\tilde{w} = \begin{cases} \frac{K(z\tilde{I}^{(0)}/\tilde{\sigma}_{\text{SEI}} - \tilde{k}^2 \text{Ca}_{\text{Li}}^{\text{SEI}})}{e^{\alpha} \cot^{2}\theta_{\alpha}^{(0)}/\tilde{k}_{0} - AB/(\tilde{D}_{+}\tilde{k}) + K\tilde{L}_{1}z/\tilde{\sigma}_{\text{SEI}}}, & \text{underlimiting,} \\ \frac{K(z\tilde{I}^{(0)}/\tilde{\sigma}_{\text{SEI}} - \tilde{k}^2 \text{Ca}_{\text{Li}}^{\text{SEI}})}{e^{\alpha} \cot^{2}\theta_{\alpha}^{(0)}/\tilde{k}_{0} - AK/(\tilde{D}_{+}\tilde{k}\tilde{c}_{+}^{(0)}) + K\tilde{L}_{1}z/\tilde{\sigma}_{\text{SEI}}} \end{cases} & \text{overlimiting,} \end{cases}$$

that involve non-dimensional wavenumber  $\tilde{k}$ , current density  $\tilde{I}^{(0)}$ , SEI ionic conductivity and thickness  $\tilde{\sigma}_{SEI}$  and  $\tilde{L}_{1}$ , Li<sup>+</sup> diffusion coefficient in the electrolyte  $\tilde{D}_{+}$ , reaction rate constant  $\tilde{k}_{0}$  and capillary number that is related to the interfacial energy between SEI and Li-metal Ca $_{\rm Li}^{\rm SEI} = \frac{\omega \gamma_{\rm Li}^{\rm SEI}}{RTL}$ . The base-state variables  $\tilde{c}_{+}^{(0)}(\tilde{\xi})$  and  $\tilde{\phi}^{(0)}(\tilde{\xi})$ , along with  $e^{\alpha_{\rm cat}z\tilde{\eta}_{\alpha}^{(0)}}$  and coefficients A, B, and K, are defined in Eqs. B.12, B.3, B.9c and B.7b, and evaluated at  $\tilde{\xi} = \tilde{L}_{1}$ . For both underlimiting and overlimiting conditions, the critical wavenumber  $\tilde{k}_{\rm cri}$ , defined as the threshold beyond which the perturbations are stabilized and the interface becomes stable, is given by

$$\tilde{k}_{\text{cri}} = \sqrt{\frac{z\tilde{I}^{(0)}}{\tilde{\sigma}_{\text{SEI}} \text{Ca}_{\text{Li}}^{\text{SEI}}}}.$$
 [19]

Figure 4 presents a comparison between the numerical and analytical dispersion relations for both underlimiting ( $\phi_e = -0.1~V$ ) and overlimiting ( $\phi_e = -2~V$ ) conditions, with the presence of a SEI layer. Since the numerical simulations are performed under a constant applied voltage, we first solve the base-state Eqs. numerically (Appendix A). Using the base-state variables  $\tilde{c}_{\pm}^{(0)}(\tilde{\xi})$  and  $\tilde{\phi}^{(0)}(\tilde{\xi})$ , we calculate the current density  $\tilde{I}^{(0)}$ , which is then used in the analytical dispersion relations. As shown in Fig. 4, the numerical and analytical solutions are virtually indistinguishable for both underlimiting and overlimiting current conditions. This confirms that the analytical model accurately captures the dispersion relations and can reliably predict the critical wavenumber  $\tilde{k}_{cri}$ .

We also derive analytical expressions for the dispersion relations in the absence of a SEI layer, considering both underlimiting and overlimiting current conditions:

$$\tilde{w} = \begin{cases} \frac{B\tilde{I}^{(0)}/(2\tilde{D}_{+}) - K\tilde{k}^{2}Ca_{Li}^{el}}{e^{\alpha_{cat}\tilde{v}\tilde{\eta}_{\alpha}^{(0)}}/\tilde{k}_{0} - AB/(\tilde{D}_{+}\tilde{k})} & \text{underlimiting,} \\ \frac{K(d\tilde{\phi}^{(0)}/d\tilde{\xi} - \tilde{k}^{2}Ca_{Li}^{el})}{e^{\alpha_{cat}\tilde{v}\tilde{\eta}_{\alpha}^{(0)}}/\tilde{k}_{0} - AK/(\tilde{D}_{+}\tilde{k}\tilde{c}_{+}^{(0)})} & \text{overlimiting.} \end{cases}$$
[20]

These relations depend on the non-dimensional wavenumber  $\tilde{k}$ , the current density  $\tilde{I}^{(0)}$ , the Li<sup>+</sup> diffusion coefficient  $\tilde{D}_+$ , and the capillary number  $\operatorname{Ca^{el}_{Li}}$  (which characterizes the interfacial energy between the electrolyte and Li-metal) as well as the reaction parameter  $\tilde{k}_0$ ;  $\mathrm{e}^{\alpha_{\mathrm{cut}} z \tilde{l}_{\alpha}^{(0)}}$  is defined in Eq. B.12; the base-state quantities,  $\tilde{c}_+^{(0)}$ ,  $\tilde{\phi}^{(0)}$ , and  $\partial \tilde{\phi}^{(0)}/\partial \tilde{\xi}$  are given in Eqs. B.3 and B.9c for underlimiting and overlimiting conditions, respectively, and evaluated at  $\tilde{\xi}=0$ . The corresponding critical wavenumbers are:

$$\tilde{k}_{\text{cri}} = \begin{cases} \sqrt{\frac{\tilde{I}^{(0)}}{2\tilde{D}_{+}\tilde{c}^{\Theta}K} \operatorname{Ca}_{\text{Li}}^{\text{el}}} + \frac{\tilde{I}^{(0)}}{\operatorname{Ca}_{\text{Li}}^{\text{el}}(2\tilde{D}_{+} - \tilde{I}^{(0)})} & \text{underlimiting,} \\ \sqrt{\frac{z}{\tilde{\lambda}_{\text{D}}} \operatorname{Ca}_{\text{Li}}^{\text{el}}} \left( \frac{\tilde{I}^{(0)}}{\tilde{D}_{+}} - 2 \right)^{1/2} & \text{overlimiting,} \end{cases}$$
[21]

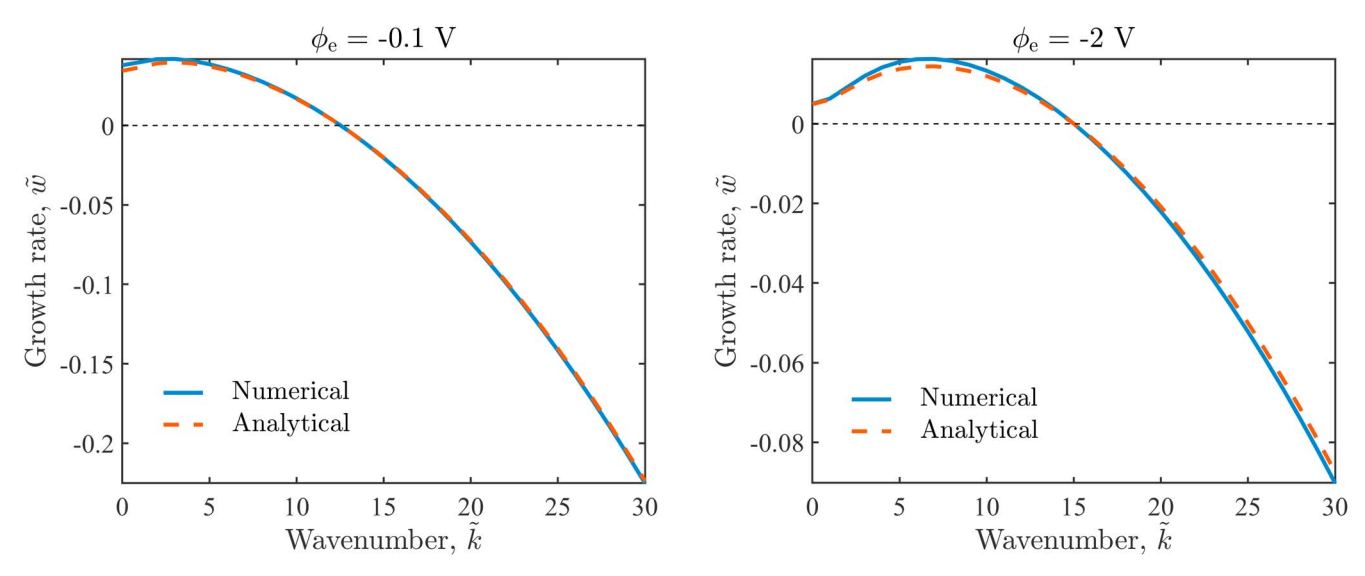


Figure 4. Comparison of numerical and analytical dispersion relations under underlimiting ( $\phi_e = -0.1 \ V$ ) and overlimiting conditions ( $\phi_e = -2 \ V$ ) in the presence of a SEI layer.

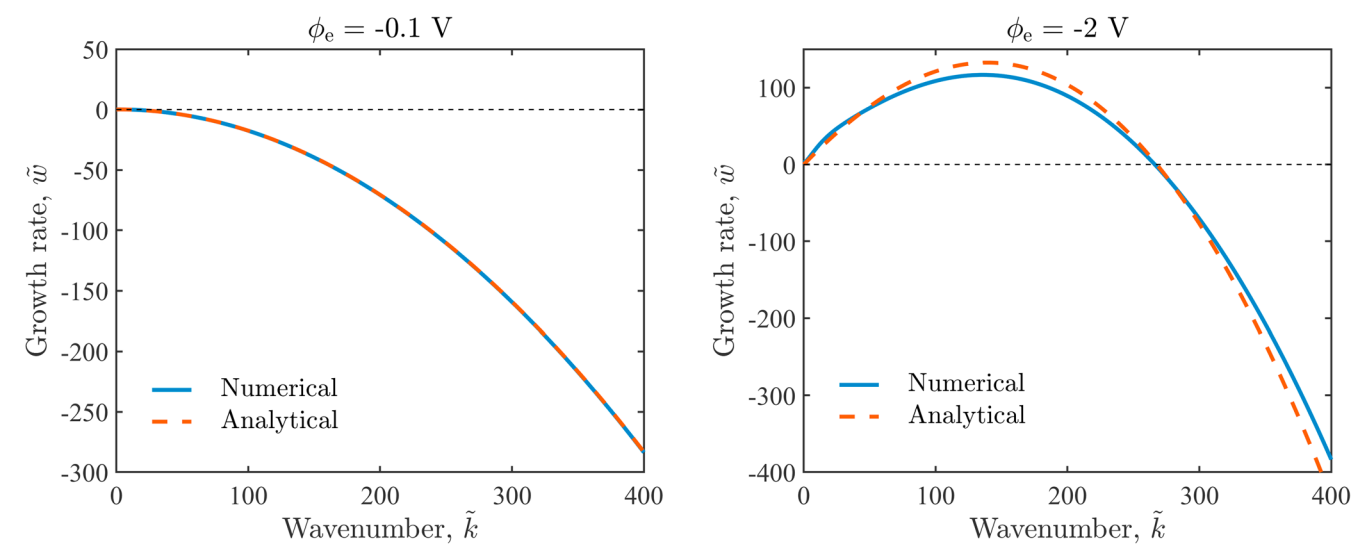


Figure 5. Comparison of numerical and analytical dispersion relations under underlimiting ( $\phi_e = -0.1 \ V$ ) and overlimiting conditions ( $\phi_e = -2 \ V$ ) in the absence of a SEI layer.

where  $\tilde{\lambda}_D = \sqrt{\frac{RTe}{2L^2F^2c_0}}$  is the Debye length. Figure 5 shows a comparison between numerical and analytical dispersion relations for underlimiting ( $\phi_e = -0.1~V$ ) and overlimiting ( $\phi_e = -2~V$ ) conditions in the absence of a SEI layer. Figure 5 demonstrates that the numerical and analytical solutions are virtually indistinguishable for both underlimiting and overlimiting conditions, with the critical wavenumber  $\tilde{k}_{cri}$  accurately captured.

We next construct stability diagrams using the analytical expressions for the critical wavenumber  $\tilde{k}_{cri}$  with and without SEI, as given in Eqs. 19 and 21. We set  $\sigma_{ref} = \sigma_{SEI}$  to non-dimensionalize the model parameters and current density and explore the influence of SEI properties on dendrite suppression in the non-dimensional phase space. These stability diagrams elucidate how SEI-electrolyte dyads affect the morphological stability of the Li-electrolyte interface. Figure 6 presents stability diagrams under underlimiting conditions, spanned by two non-dimensional ratios: SEI ionic conductivity to electrolyte cation diffusivity,  $\tilde{\sigma}_{SEI}/\tilde{D}_+$ , Li/SEI to Li/electrolyte capillary number (interfacial energy) ratio, Ca $_{Li}^{SEI}/Ca_{Li}^{el}$ , across various current densities,  $\tilde{I}^{(0)} = 1.9 \times 10^{-3}$ ,  $1.9 \times 10^{-2}$  and  $1.9 \times 10^{-1}$ . The

solid blue lines indicate the stability boundaries where the critical wavenumbers,  $\tilde{k}_{cri}$ , are equal with and without the SEI. To the right of these boundaries (blue-shaded region), the SEI contributes a stabilizing effect ( $\tilde{k}_{cri}$  is lower with SEI than without); to the left, it has a destabilizing effect. The dash-dotted black lines represent the limiting current density  $\tilde{I}_{\text{lim}}^{(0)} = 2\tilde{D}_{+}$ , above which the underlimiting assumptions break down due to cation depletion  $(\tilde{c}_+ \to 0)$  predicted by Eq. B.3. These results show that a SEI with high interfacial energy with Li and high ionic conductivity effectively suppresses dendrite growth. The benefit of SEI is especially pronounced when the electrolyte exhibits low cation diffusivity and low interfacial energy with Li. It is important to note that this does not imply that such an electrolyte alone offers better stability; rather, it highlights that the addition of a SEI significantly improves stability in systems that are otherwise more prone to instability. We further elucidate the effects of SEI-electrolyte pairings. While high ionic conductivity and interfacial energy with Li in the SEI are generally favorable for enhancing interfacial stability, these ideal properties may not always be achievable in practice. In such cases, even a SEI with low conductivity or interfacial energy can still help suppress dendrites in systems when the

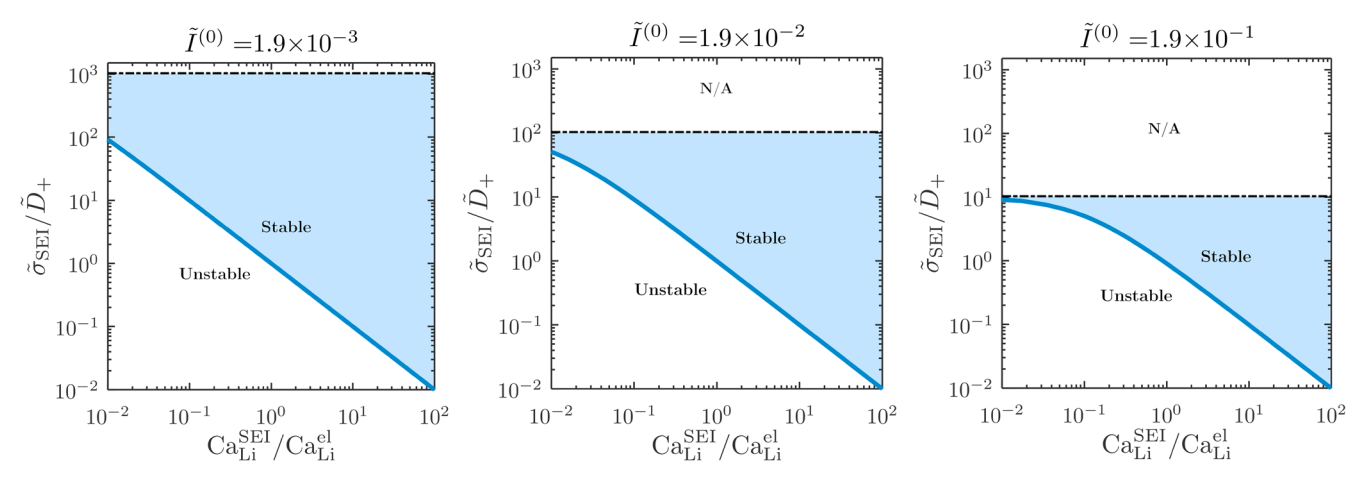


Figure 6. Stability diagrams under underlimiting conditions in the non-dimensional phase space of SEI ionic conductivity to electrolyte cation diffusivity ratio,  $\tilde{\sigma}_{\text{SEI}}/\tilde{D}_{+}$ , and interfacial energy (capillary number) ratio, Ca  $_{\text{Li}}^{\text{SEI}}/\text{Ca}_{\text{Li}}^{\text{el}}$ , for various current densities  $\tilde{I}^{(0)} = 1.9 \times 10^{-3}$ ,  $1.9 \times 10^{-2}$ ,  $1.9 \times 10^{-1}$ . Solid blue lines mark stability boundaries where the critical wavenumbers  $\tilde{k}_{\text{cri}}$  are equal with and without SEI. To the right (blue-shaded region), the SEI stabilizes the interface; to the left, it destabilizes it. Dash-dotted black lines indicate the limiting current density  $\tilde{I}_{\text{lim}}^{(0)} = 2\tilde{D}_{+}$ , above which underlimiting assumptions break down due to electrolyte depletion ( $\tilde{c}_{+} \to 0$ ).

electrolyte has lower cation diffusivity or interfacial energy with Li. Conversely, when the electrolyte exhibits high diffusivity or interfacial energy, the SEI must also possess correspondingly high ionic conductivity and interfacial energy with Li to maintain stability. These findings highlight the importance of tailoring SEI properties in response to the specific electrolyte characteristics to optimize dendrite suppression.

Figure 7 displays the stability diagrams under overlimiting current conditions in the non-dimensional phase space of  $Ca_{Li}^{SEI}/(\tilde{\lambda}_D Ca_{Li}^{el})$  versus  $\tilde{\sigma}_{SEI}/\tilde{D}_+$  for various current densities,  $\tilde{I}^{(0)} = 9.7 \times 10^2$ ,  $9.7 \times 10^3$  and  $9.7 \times 10^4$ . The dashed red lines separate the stable (red-shaded) and unstable regions, where the inclusion of a SEI layer stabilizes or destabilizes the interface, respectively. The dash-dotted black lines again represent the limiting current density  $\tilde{I}_{\text{lim}}^{(0)} = 2\tilde{D}_{+}$ ; below these lines, the overlimiting assumptions break down as the cation concentration  $\tilde{c}_+$  diverges according to Eq. B.9c. Consistent with the underlimiting diagrams, SEI layers with high ionic conductivity and high interfacial energy with Li promote interfacial stability. Under overlimiting conditions, the stability behavior is also influenced by the Debye length  $\tilde{\lambda}_{\rm D}$  of the electrolyte: a smaller Debye length (equivalent to lower permittivity  $\epsilon$ ) implies a thinner double layer and is associated with enhanced dendrite suppression. This underscores the role of local charge accumulation, as dendrite growth is exacerbated when the local charge density  $\tilde{\rho}_{\rm e}^{(0)} = \tilde{c}_+^{(0)} - \tilde{c}_-^{(0)}$  intensifies within the diffuse layer.

To compare both regimes, Fig. 8 presents stability diagrams for underlimiting and overlimiting conditions in the  $(\tilde{I}^{(0)}, \operatorname{Ca}_{I,i}^{\operatorname{SEI}}/\operatorname{Ca}_{I,i}^{\operatorname{el}})$ phase space for varying  $\tilde{\sigma}_{SEI}/\tilde{D}_{+}$ . The dash-dotted lines indicate the boundaries between underlimiting and overlimiting regimes at  $\tilde{I}_{\text{lim}}^{(0)} = 2\tilde{D}_{+}$ . Analytical expressions for the critical wavenumber  $k_{\text{cr}}$ are used here; however, more accurate predictions near the transition regime could be obtained using numerical solutions. The blue and red shaded regions indicate parameter combinations where the inclusion of a SEI layer stabilizes the interface compared to the no-SEI scenario. A high interfacial energy ratio Ca SEI/Cael or larger SEI ionic conductivity to electrolyte diffusivity ratio  $\tilde{\sigma}_{SEI}/\tilde{D}_{+}$  enlarges the stable regions for both current conditions and a high current density  $\tilde{I}^{(0)}$  also expands the stable regions for underlimiting conditions. However, under overlimiting conditions, a larger current density  $\tilde{I}^{(0)}$  shrinks the stable regions, as reflected in the scaling behavior of the critical wavenumbers:  $\tilde{k}_{\rm cri} \propto \tilde{I}^{1/2}$  with a SEI layer and  $\tilde{k}_{\rm cri} \propto \tilde{I}^{1/4}$  without SEI. When transitioning from underlimiting to overlimiting regimes, the overall stability regions expand. Under low-current (underlimiting) conditions, stabilization requires a SEI with high interfacial energy, while at high-current (overlimiting) conditions, even a small

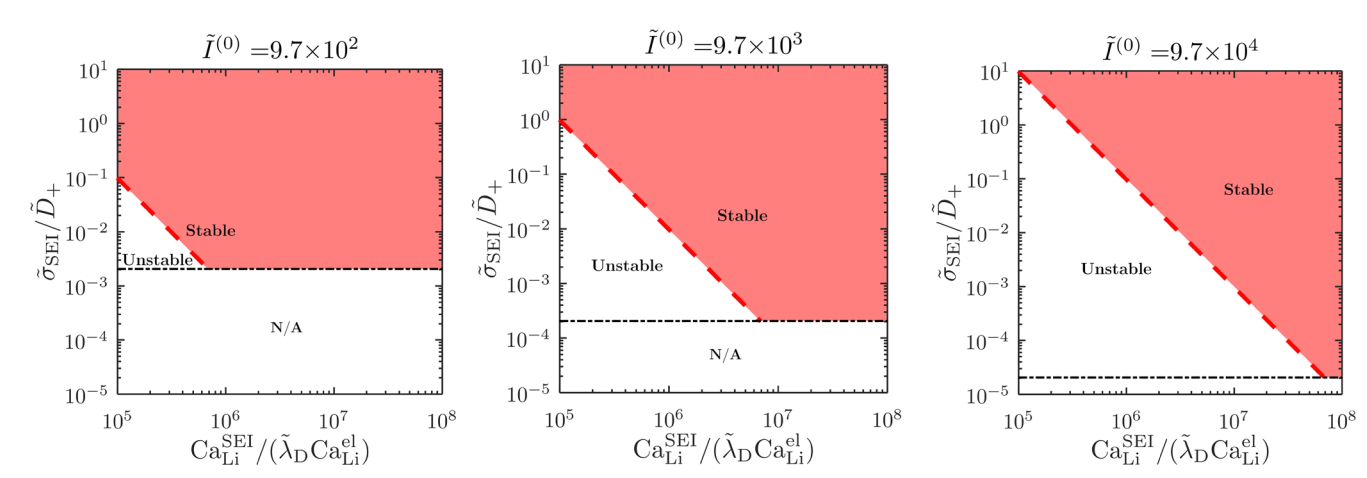
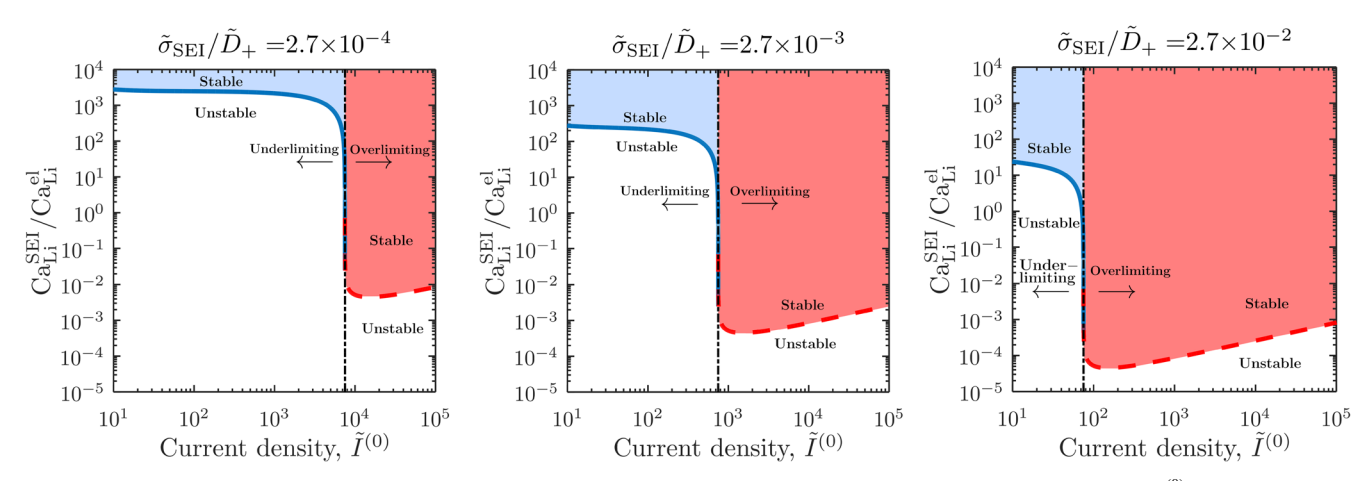


Figure 7. Stability diagrams under overlimiting conditions in the non-dimensional space of  $Ca_{\rm Li}^{\rm EI}/(\tilde{l}_{\rm D}Ca_{\rm el}^{\rm cl})$  versus  $\tilde{\sigma}_{\rm SEI}/\tilde{D}_{+}$  for current densities  $\tilde{I}^{(0)}=9.7\times10^2,\,9.7\times10^3,\,9.7\times10^3,\,9.7\times10^4$ . Dashed red lines separate stable (red-shaded) and unstable regions, where the SEI layer suppresses or promotes dendrite growth, respectively. Dash-dotted black lines mark  $\tilde{I}_{\rm lim}^{(0)}=2\tilde{D}_{+}$ , below which the overlimiting assumptions are invalid due to divergence in  $\tilde{c}_{+}$ .



**Figure 8.** Stability diagrams combining underlimiting and overlimiting regimes in the non-dimensional phase space of current density  $\tilde{I}^{(0)}$  and interfacial energy ratio  $Ca_{Li}^{SEI}/Ca_{Li}^{el}$ , for varying  $\tilde{\sigma}_{SEI}/\tilde{D}_{+} = 2.7 \times 10^{-4}$ ,  $2.7 \times 10^{-3}$ ,  $2.7 \times 10^{-2}$ . Dash-dotted lines indicate the transition at  $\tilde{I}_{lim}^{(0)} = 2\tilde{D}_{+}$ . Shaded blue and red regions represent parameter regimes where the SEI layer enhances stability relative to the no-SEI case.

interfacial energy ratio is sufficient for stabilization compared to the no-SEI case. This trend reflects the changing interfacial dynamics, where space-charge layers and non-electroneutral effects dominate under overlimiting currents. In this regime, the SEI acts as a buffer that moderates the electric field and space-charge accumulation near the anode surface, reducing the driving force for dendrite formation—even when its interfacial energy is modest. These comparison plots highlight the fundamentally different stabilization mechanisms across the two limiting current conditions and emphasize the importance of relaxing the electroneutrality assumption when studying dendrite initiation under high current densities.

Our results also quantify the impact of SEI thickness,  $\tilde{L}_1$ , on dendrite growth. According to Eq. 19, at any given current density  $\tilde{I}^{(0)}$ , the critical wavenumber  $\tilde{k}_{cri}$  is independent of  $\tilde{L}_1$ , under both underlimiting and overlimiting conditions. However,  $\tilde{L}_1$  does impact the maximum growth rate  $\tilde{w}_{max}$ , with the nonlinear dependence of the growth rate on the SEI thickness,  $\tilde{w} = \tilde{w}(\tilde{L}_1)$ , given by Eq. 18. These relations reveal a complex interplay among SEI thickness, current density, and the transport properties of both the SEI and the electrolyte. Thus, tuning SEI thickness offers an additional design parameter for improving dendrite suppression, complementing strategies that focus on transport characteristics and interfacial energy.

#### Conclusions

We investigate the impact of SEI-electrolyte dyad properties on dendrite growth in LMBs by performing a physics-based linear stability analysis of dendrite initiation. This model explicitly incorporates a SEI layer between the Li-metal anode and the electrolyte while relaxing the electroneutral assumption. Our analysis considers how SEI transport properties (e.g., ionic conductivity), thickness, and interfacial energy at the Li-SEI interface interact with electrolyte characteristics (e.g., diffusion coefficient, permittivity, and Li-electrolyte interfacial energy) and operating conditions (current density or applied voltage) to determine interfacial stability. Our key results are the analytical expressions that relate the instability growth rate of dendrite initiation to both material properties and battery operating conditions for both underlimiting and overlimiting current conditions. We derive and compare the growth rate expressions with and without the presence of a SEI layer, revealing its crucial role in dendrite suppression. Our analysis leads to the following major conclusions:

• SEI properties play a significant role in influencing both the dendrite growth rate and the critical wavenumber. Under the same current density and system parameters, a higher SEI ionic

conductivity results in a smaller critical wavenumber, indicating enhanced interfacial stabilization. While the critical wavenumber is independent of SEI thickness in both under- and overlimiting regimes, the maximum growth rate is affected by SEI thickness.

- Interfacial stability is promoted by a high dimensionless SEI ionic conductivity-to-electrolyte diffusivity ratio and a high Li/SEI-to-Li/electrolyte interfacial energy ratio. A smaller Debye length, or equivalently a lower electrolyte permittivity, implies a thinner electric double layer and improves dendrite suppression by reducing space-charge accumulation near the solid/liquid interface.
- High current density broadens the stability window in the underlimiting regime but narrows it in the overlimiting regime. These results emphasize the need to go beyond the electroneutral approximation when modeling dendrite behavior at high current densities.
- Crucially, interfacial stability is governed not by SEI properties in isolation but by SEI-electrolyte dyads—the coupled property interactions that define the stability phase space.

These findings offer several key design principles for interfacial stabilization. First, SEI transport properties and interfacial energy must be co-optimized with electrolyte properties; a SEI formulation that is effective in one electrolyte environment may be ineffective in another. Second, dendrite suppression mechanisms differ fundamentally across current regimes: dendrite initiation in underlimiting regimes is governed by ion concentration gradients, whereas overlimiting regimes are dominated by electric potential gradients and space-charge effects. Therefore, predictive design requires models that go beyond the electroneutral approximation to accurately capture dendrite behavior at high current densities.

Our results motivate the rational design of artificial SEI layers as a route to stabilize Li-metal anodes. Transport properties (ionic conductivity and diffusivity), SEI thickness, and interfacial energy with Li-metal should be treated as tunable design variables that depend on the operating regime and electrolyte environment. Future work will incorporate mechanical effects and fracture criteria to provide a more comprehensive understanding of SEI failure and dendrite propagation, ultimately enabling predictive models for next-generation, high-performance LMBs.

#### **Appendix A: Perturbation Analysis**

We introduce dimensionless variables

$$\tilde{x} = \frac{x}{L}, \quad \tilde{y} = \frac{y}{L}, \quad \tilde{t} = \frac{t\sigma_{\text{ref}}RT}{F^2c_0L^2}, \quad \tilde{c} = \frac{c}{c_0},$$
 [A.1a]

$$\tilde{\phi} = \frac{F\phi}{RT}, \quad \tilde{h} = \frac{h}{L}, \quad \tilde{w} = \frac{wF^2c_0L^2}{\sigma_{ref}RT}, \quad \tilde{\kappa} = L\kappa,$$
 [A.1b]

and model parameters.

$$\begin{split} \tilde{\sigma}_{\rm SEI} &= \frac{\sigma_{\rm SEI}}{\sigma_{\rm ref}}, \quad \tilde{D}_{\pm} = \frac{D_{\pm}F^2c_0}{\sigma_{\rm ref}RT}, \quad \tilde{c}^{\Theta} = \frac{c^{\Theta}}{c_0}, \\ \tilde{k}_0 &= \frac{LF^2k_0}{RT\sigma_{\rm ref}\gamma_{\rm ts}}, \quad \tilde{\lambda}_D^2 = \frac{RT\epsilon}{2L^2F^2c_0}. \end{split} \tag{A.1c}$$

We define also the capillary number

$$Ca_{Li}^{SEI} = \frac{\omega \gamma_{Li}^{SEI}}{RTL}, \quad Ca_{Li}^{el} = \frac{\omega \gamma_{Li}^{el}}{RTL},$$
 [A.1d]

and the normalized interfacial current density

$$\tilde{I} = \frac{ILF}{zRT\sigma_{ref}},$$
 [A.1e]

where  $\gamma_{\rm Li}^{\rm el}$  is the isotropic interfacial energy of the Li-metal with the liquid electrolyte (J/m²). Unless specified otherwise, all notations will be dimensionless even if we drop the tildes. Substituting Eq. 15 into the dimensionless form of Eqs. 1–14, and collecting the terms of order  $\varepsilon^0$  and  $\varepsilon^1$  leads to the base-state and perturbed-state BVPs. The boundary conditions on the evolving electrode surface,  $\Gamma_{\rm in}(t)$ , represented by points  $(y,h(y,t))^{\rm T}$ , are derived by approximating the values of  $\phi_{\rm SEI}(\mathbf{x} \in \Gamma_{\rm in},t)$ ,  $c_{\pm}(\mathbf{x} \in \Gamma_{\rm in},t)$ , and their gradients. This approximation is performed by expanding these quantities using a Taylor series around the base state  $\Gamma_{\rm in}^{(0)} = \mathbf{x} = (x,y)^{\rm T}$ :  $x = h^{(0)}$ ,  $0 \le y \le B$ . Full details of this expansion can be found in Ref. 3. The current density I is expanded to first order,  $I = I^{(0)} + \hat{\varepsilon}I^{(1)}$ , the components  $I^{(0)}$  and  $I^{(1)}$  are given by Eq. A.2c.

We rewrite the BVPs in terms of a moving coordinate system associated with the electrode-electrolyte interface ( $\xi \equiv x - Ut, y$ ) as the interface  $h^{(0)}(t)$  moves with velocity  $U = dh^{(0)}/dt = \omega t^{(0)}$ . The linear stability analysis applies to the early stages of dendrite formation, where  $Ut \ll L_1$  and, given that  $L_1 \ll 1$ , we have  $Ut \ll 1$ .

**A.0.1.** Solid-electrolyte interphase (SEI).—The base-state and perturbed-state dependent variables  $\phi_{\rm SEI}^{(0)}(\xi)$  and  $\phi_{\rm SEI}^{(1)}(\xi)$  in the SEI satisfy the one-dimensional Laplace equations,

$$i_{\rm SEI}^{(n)} = -\sigma_{\rm SEI} \frac{{\rm d}\phi_{\rm SEI}^{(n)}}{{\rm d}\xi}, \quad \frac{{\rm d}i_{\rm SEI}^{(n)}}{{\rm d}\xi} = 0,$$
 $n = 0, 1; \quad 0 < \xi < L_1,$  [A.2a]

where  $i_{SEI} = |\mathbf{i}_{SEI}|$  and  $\mathbf{i}_{SEI}^{(n)} = (i_{SEI}^{(n)}, 0)^{\mathsf{T}}$  for n = 0, 1, These Eqs. are subject to boundary conditions

$$-i_{\text{SEI}}^{(n)}(0) = I^{(n)}, \quad \phi_{\text{SFI}}^{(n)}(L_1) = \phi_{\text{el}}^{(n)}(L_1), \quad n = 0, 1;$$
 [A.2b]

with

where  $\eta_a^{(0)} = \phi_e - \phi_{\rm SEI}^{(0)} - E^{\Theta}$  and  $c_+^{(0)}(0) = c_+^{(0)}(L_{\rm I})$  as we assume a constant cation concentration in the SEI.  $\hat{\phi}_{\rm SEI}^{(1)}$  is the Taylor series expansion of  $\phi_{\rm SEI}(\mathbf{x} \in \Gamma_{\rm in})$  around the base state  $\Gamma_{\rm in}^{(0)}$ ,

$$\hat{\phi}_{\rm SEI}^{(1)} = h^{(1)} \frac{{\rm d}\phi_{\rm SEI}^{(0)}}{{\rm d}\xi} + \varphi_{\rm SEI}^{(1)}, \quad \hat{c}_{+}^{(1)} = h^{(1)} \frac{{\rm d}c_{+}^{(0)}}{{\rm d}\xi} + c_{+}^{(1)}. \quad [\text{A}\cdot3]$$

In Equation A.2b, we employ this expansion such that  $i_{\rm SEI}^{(1)} = -\sigma_{\rm SEI} {\rm d}\hat{\phi}_{\rm SEI}^{(1)}/{\rm d}\xi$ . It follows from Eqs. 12, 15 and 16 that

$$wh^{(1)} = \omega c_0 I^{(1)}.$$
 [A·4]

**A.0.2.** Liquid electrolyte.—The base-state and perturbed-state dependent variables  $c_{\pm}^{(0)}(\xi)$ ,  $\phi^{(0)}(\xi)$ ,  $c_{\pm}^{(1)}(\xi)$  and  $\phi^{(1)}(\xi)$  satisfy the one-dimensional differential equations

$$-\frac{\mathrm{d}J_{\pm}^{(n)}}{\mathrm{d}\xi} = n(w + k^2 D_{\pm}) c_{\pm}^{(1)} + n D_{\pm} z_{\pm} k^2 \phi^{(1)} c_{\pm}^{(0)}, \tag{A.5a}$$

$$-\frac{\mathrm{d}^2 \phi^{(n)}}{\mathrm{d}\xi^2} = \frac{z_+ c_+^{(n)} + z_- c_-^{(n)}}{2\lambda_D^2} - nk^2 \phi^{(1)},$$

$$n = 0, 1; \quad L_1 < \xi < 1, \tag{A.5b}$$

where

$$J_{\pm}^{(n)} = -D_{\pm} \left( \frac{\mathrm{d} c_{\pm}^{(n)}}{\mathrm{d} \xi} + z_{\pm} j_{\phi}^{(0)} c_{\pm}^{(n)} + n z_{\pm} c_{\pm}^{(0)} j_{\phi}^{(1)} \right), \quad j_{\phi}^{(n)} \equiv \frac{\mathrm{d} \phi^{(n)}}{\mathrm{d} \xi}.$$
[A.5c]

Eqs A.5a-A.5c are subject to the boundary conditions at  $\xi = L_1$ ,

$$\frac{\mathrm{d}c_{+}^{(n)}}{\mathrm{d}\xi} = 0, \quad J_{-}^{(n)} = 0, \quad J_{+}^{(n)} = i_{\mathrm{SEI}}^{(n)}, \quad n = 0, 1;$$
 [A.5d]

and at  $\xi = 1$ ,

$$\phi^{(n)}(1) = 0, \quad c_{+}^{(n)}(1) = c_{-}^{(n)}(1) = \begin{cases} 1, & n = 0; \\ 0, & n = 1; \end{cases}$$
 [A.5e]

We solve the base-state Eqs. A2 and A5 with n=0 in the SEI and liquid electrolyte numerically with the Matlab function pdepe to obtain  $c_{\pm}^{(0)}(\xi)$ ,  $\phi^{(0)}(\xi)$ , and their first- and second-order derivatives. These are then used as coefficients in the perturbed-state Eqs. A2 and A5 with n=1. We employ a second-order finite-difference scheme<sup>3</sup> and obtain the resulting generalized eigenvalue problem,

$$Y\nu = wZ\nu, \quad \nu = [h^{(1)}, \ c_{\pm,1}^{(1)}, \ \phi_1^{(1)}, \ c_{\pm,2}^{(1)}, \ \phi_2^{(1)}, ..., \ c_{\pm,N}^{(1)}, \ \phi_N^{(1)}]^T, \label{eq:energy}$$
 [A·6]

which is subsequently solved with the Matlab function eigs to compute the dispersion relation w = w(k). Moreover, we derive the conditions for interfacial stability both with and without the

$$I^{(n)} = k_0 e^{-\alpha_{\text{cat}} z \eta_a^{(0)}} \begin{cases} (c_+^{(0)}/c^{\Theta} - e^{z \eta_a^{(0)}}) & n = 0 \\ \left\{ \frac{\hat{c}_+^{(1)}}{c_+^{\Theta}} + \left[ (1 - \alpha_{\text{cat}}) e^{z \eta_a^{(0)}} + \alpha_{\text{cat}} \frac{c_+^{(0)}}{c^{\Theta}} \right] (z \hat{\phi}_{\text{SEI}}^{(1)} - k^2 \text{Ca}_{\text{Li}}^{\text{SEI}} h^{(1)}) \right\} & n = 1 \end{cases},$$
 [A.2c]

inclusion of a SEI layer; these conditions are obtained analytically in Appendix  $\, B \,$ .

#### Appendix B: Analytical Stability Criteria

We obtain the analytical expression of the spatial distribution of the electric potential in the SEI layer by solving the BVPs described in Eqs. A.2a-A.2b

$$\phi_{\text{SEI}}^{(n)}(\xi) = \frac{I^{(n)}}{\sigma_{\text{SEI}}}(\xi - L_1) + \phi_{\text{el}}^{(n)}(L_1), \quad n = 0, 1.$$
 [B·1]

**B.1.** Underlimiting current conditions.—Under low current density, the electrolyte is locally electroneutral, we have,  $c = c_+ = c_- = e^{z\phi}$ , that satisfies mass conservation in the electrolyte (Eq. 2) and boundary condition in Eq. 14. Employing the perturbations of  $c_{\pm}$  and  $\phi$  in Eq. 15 and applying Taylor series expansion yields

$$c_{\perp}^{(0)} = e^{z\phi^{(0)}}, \quad c^{(1)} = z\phi^{(1)}e^{z\phi^{(0)}}.$$
 [B·2]

We then solve the base-state Eqs. in A.5a with n = 0,

$$c_{+}^{(0)} = \frac{I^{(0)}}{2D_{+}}(\xi - 1) + 1, \quad \phi^{(0)} = \ln\left[\frac{I^{(0)}}{2D_{+}}(\xi - 1) + 1\right], \quad L_{1} < \xi < 1.$$
[B·3]

Under local electroneutrality and assuming that  $w \ll Dk^2$  in Eq. A.5a with n=1, i.e., that the temporal fluctuations of the first-order perturbation  $c_+^{(1)}(\xi)$  are negligible, the perturbed-state Eq. A.5a reduces to

$$\frac{\mathrm{d}^2 c_+^{(1)}}{\mathrm{d}\xi^2} = k^2 c_+^{(1)}, \quad L_1 < \xi < 1,$$
 [B·4]

whose solution is  $c_+^{(1)}(\xi) = \beta_1 \exp(k\xi) + \beta_2 \exp(-k\xi)$ . The constants of integration  $\beta_1$  and  $\beta_2$  are obtained from the boundary condition in Eq. A.5e with n = 1,

$$c_{\perp}^{(1)} = 1, \quad \xi = 1,$$
 [B·5]

and by combining Eqs. B.1–B.3 with Eq. A.2c and substituting the resulting equation to the boundary condition in Eq. A.5d with n = 1,

$$zD_{+}\left(\frac{\mathrm{d}\phi^{(0)}}{\mathrm{d}\xi}c_{+}^{(1)} + c_{+}^{(0)}(L_{1})\frac{\mathrm{d}\phi^{(1)}}{\mathrm{d}\xi}\right) = I^{(1)}.$$
 [B·6]

We then employ this solution  $c_+^{(1)}$  in Eq. A.4 and obtain the dispersion relation

$$w = \frac{K(zI^{(0)}/\sigma_{SEI} - k^2Ca_{Li}^{SEI})}{e^{\alpha_{cat}z\eta_{\alpha}^{(0)}}/k_0 - AB/(D_+k) + KL_1z/\sigma_{SEI}}$$
[B.7a]

with

**B.2.** Overlimiting current conditions.—Under high current density, as the electric potential gradient is large close to the liquid/solid interface, we assume  $\frac{\mathrm{d}^2\phi^{(1)}}{\mathrm{d}\xi^2}$  and  $k^2\phi^{(1)}$  dominate in Eq. A.5b,

$$\frac{\mathrm{d}^2 \phi^{(1)}}{\mathrm{d}\xi^2} = k^2 \phi^{(1)}, \quad L_1 < \xi < 1,$$
 [B.9a]

whose solution is  $\phi^{(1)}(\xi) = \zeta_1 \exp(k\xi) + \zeta_2 \exp(-k\xi)$ . In Eq. A.5a with n=1, we assume  $\frac{dc_+^{(1)}}{d\xi}$  and  $z_+j_\phi^{(0)}c_+^{(1)}$  are negligible compared to  $z_+c_+^{(0)}j_\phi^{(1)}$ , the boundary condition  $J_+^{(1)}=i_{\rm SEI}^{(1)}$  in Eq. A.5d can be written as

$$I^{(1)} = z_+ c_+^{(0)} (L_1) \frac{\mathrm{d}\phi^{(1)}}{\mathrm{d}\xi},$$
 [B.9b]

where we adopt the analytical expression for base-state  $c_+^{(0)}$  and  $\frac{\mathrm{d}\phi^{(0)}}{\mathrm{d}\xi}$  in Ref. 35 under overlimiting condition,

$$c_{+}^{(0)} = \frac{\lambda_{\rm D} \sqrt{I^{(0)}/D_{+}}}{z\sqrt{1 - \xi - 2D_{+}/I^{(0)}}},$$

$$\frac{\mathrm{d}\phi^{(0)}}{\mathrm{d}\xi} = \frac{I^{(0)}}{D_{+}zc_{+}^{(0)}}, \quad L_{1} < \xi < 1.$$
 [B.9c]

The constants of integration  $\zeta_1$  and  $\zeta_2$  are obtained from boundary condition in A.5e with n=1,

$$\phi^{(1)} = 0, \quad \xi = 1,$$
 [B.9d]

and by substituting Eq. B.1 into Eq. A.2c with n=1 while ignoring the diffusion contribution in  $I^{(1)}$  and combining the resulting equation with Eq. B.9b. We employ this solution in Eq. A.4 and the resulting dispersion relation is

$$w = \frac{K(zI^{(0)}/\sigma_{\rm SEI} - k^2 {\rm Ca_{Li}^{SEI}})}{{\rm e}^{\alpha_{\rm cat}z\eta_{\alpha}^{(0)}}/k_0 - AK/(D_+kc_+^{(0)}(L_1)) + KL_1z/\sigma_{\rm SEI}}, \qquad [\text{B}\cdot 10]$$

with K and A given in Eq. B.7b. The critical wavenumber,  $k_{\rm cri}$  under high current density is

$$k_{\text{cri}} = \sqrt{\frac{zI^{(0)}}{\sigma_{\text{SEI}}\text{Cal}_{1}^{\text{SEI}}}}.$$
 [B·11]

When  $\alpha_{\text{cat}} = 0.5$ , Eq. A.2c with n = 0 can be solved for  $e^{\alpha_{\text{cat}}z\eta_a^{(0)}}$ , yielding an expression in terms of  $c_+^{(0)}(L_1)$ ,  $k_0$ ,  $c^{\Theta}$ , and  $I^{(0)}$ ,

$$K = (1 - \alpha_{\text{cat}})e^{z\eta_{\alpha}^{(0)}} + \alpha_{\text{cat}}\frac{c_{+}^{(0)}(L_{1})}{c^{\Theta}}, \quad A = \frac{e^{kL_{1}} - e^{(2-L_{1})k}}{e^{kL_{1}} + e^{(2-L_{1})k}}, \quad B = \frac{1}{c^{\Theta}} + \frac{K}{c_{+}^{(0)}(L_{1})}.$$
 [B.7b]

The critical wavenumber,  $k_{cri}$ , is a wavenumber k for which w = 0. It follows from Eq. B.7a that

$$k_{\text{cri}} = \sqrt{\frac{zI^{(0)}}{\sigma_{\text{SFI}}Ca_{\text{Li}}^{\text{SEI}}}}.$$
 [B·8]

$$\mathrm{e}^{\alpha_{\mathrm{cat}}\eta_{\alpha}^{(0)}} = \frac{\sqrt{4k_0^2\,c_+^{(0)}(L_1)/c^\Theta + I^{(0)\,2}}\,-I^{(0)}}{2k_0}. \tag{B-12}$$

**B.3.** Without SEI.—We also derive the analytical expressions for the dispersion relations under low and high current conditions in the absence of a SEI layer. By setting  $L_1 = 0$  and expanding  $\phi(\mathbf{x} \in \Gamma_{\text{in}}, t)$ ,  $c_{\pm}(\mathbf{x} \in \Gamma, t)$ , and their gradients in a Taylor series around the base state  $\Gamma_{\text{in}}^{(0)} = {\mathbf{x} = (x, y)^T : x = h^{(0)}, 0 < y < B},^3$  and following a derivation similar to the case with SEI, we obtain the dispersion relation for underlimiting current conditions,

$$w = \frac{BI^{(0)}/(2D_{+}) - Kk^{2}\text{Ca}_{\text{Li}}^{\text{el}}}{e^{\alpha_{\text{cat}}z\eta_{\alpha}^{(0)}}/k_{0} - AB/(D_{+}k)},$$
 [B·13]

and for overlimiting current conditions,

$$w = \frac{K(\mathrm{d}\phi^{(0)}/\mathrm{d}\xi - k^2 \mathrm{Ca}_{\mathrm{Li}}^{\mathrm{el}})}{\mathrm{e}^{\alpha_{\,\mathrm{cat}}z\eta_{\alpha}^{(0)}}/k_0 - AK/(D_+kc_+^{(0)}(0))},$$
 [B·14]

The base-state quantities  $c_{+}^{(0)}$ ,  $\phi^{(0)}$ , and  $d\phi^{(0)}/d\xi$ , along with  $e^{\alpha_{\rm cat} z \bar{\eta}_{\alpha}^{(0)}}$ , which appear in the dispersion relations in Eqs. B.13 and B.14, as well as in the coefficients A, B, and K (defined in Eq. B.7b), are given by Eqs. B.3 and B.9c for the underlimiting and overlimiting current conditions and Eq. B.12, and are evaluated at  $\xi=0$ . The critical wavenumbers  $k_{\rm cri}$  are

$$k_{\text{cri}} = \begin{cases} \sqrt{\frac{I^{(0)}}{2D_{+}c^{\Theta}K} \operatorname{Ca}_{\text{Li}}^{\text{el}} + \frac{I^{(0)}}{\operatorname{Ca}_{\text{Li}}^{\text{el}}(2D_{+} - I^{(0)})}} & \text{underlimiting,} \\ \sqrt{\frac{z}{\lambda_{\text{D}} \operatorname{Ca}_{\text{Li}}^{\text{el}}} \left(\frac{I^{(0)}}{D_{+}} - 2\right)^{1/2}} & \text{overlimiting.} \end{cases}$$
 [B·15]

#### **ORCID**

Weiyu Li https://orcid.org/0000-0002-7857-8115

#### References

- P. Bai, J. Li, F. R. Brushett, and M. Z. Bazant, "Transition of lithium growth mechanisms in liquid electrolytes." *Energy Environ. Sci.*, 9, 3221 (2016).
- D. Lin, Y. Liu, and Y. Cui, "Reviving the lithium metal anode for high-energy batteries." *Nat. Nanotechnol.*, 12, 194 (2017).
- W. Li, H. A. Tchelepi, Y. Ju, and D. M. Tartakovsky, "Stability-guided strategies to mitigate dendritic growth in lithium-metal batteries." *J. Electrochem. Soc.*, 169, 060536 (2022).
- C. W. Monroe and J. Newman, "The impact of elastic deformation on deposition kinetics at Li/polymer interfaces." *J. Electrochem. Soc.*, 152, A396 (2005).
- L. T. Gao and Z.-S. Guo, "Effects of optimized electrode surface roughness and solid electrolyte interphase on Li dendrite growth." *Energy Technology*, 9, 2000968 (2021).
- A. Wang, S. Kadam, H. Li, S. Shi, and Y. Qi, "Review on modeling of the anode solid electrolyte interphase (SEI) for Li-ion batteries." npj Computational Materials, 4, 15 (2018).
- J. Tarascon and M. Armand, "Issues and challenges facing rechargeable lithium batteries." Nature, 414, 359 (2001).
- W. Liu, P. Liu, and D. Mitlin, "Review of emerging concepts in SEI analysis and artificial SEI membranes for Li, sodium, and potassium metal battery anodes." Adv. Energy Mater., 10, 2002297 (2020).
- N. Gauthier, C. Courréges, J. Demeaux, C. Tessier, and H. Martinez, "Probing the in-depth distribution of organic/inorganic molecular species within the SEI of LTO/ NMC and LTO/LMO batteries: a complementary ToF-SIMS and XPS study." Appl. Surf. Sci. 501 144266 (2020)
- H. Adenusi, G. A. Chass, S. Passerini, K. V. Tian, and G. Chen, "Lithium batteries and the solid electrolyte interphase (SEI)—progress and outlook." *Adv. Energy Mater.*, 13, 2203307 (2023).
- E. Peled and S. Menkin, "Review—SEI: past, present and future." J. Electrochem. Soc., 164, A1703 (2017).
- Z. Yu, Y. Cui, and Z. Bao, "Design principles of artificial solid electrolyte interphases for lithium-metal anodes." *Cell Reports Physical Science*, 1, 100119 (2020).
- S. Park, R. Chaudhary, S. A. Han, H. Qutaish, J. Moon, M.-S. Park, and J. H. Kim, "Ionic conductivity and mechanical properties of the solid electrolyte interphase in Li metal batteries." *Energy Materials*, 3, 300005 (2023).

- G. Liu and W. Lu, "A model of concurrent Li dendrite growth, SEI growth, SEI penetration and regrowth." J. Electrochem. Soc., 164, A1826 (2017).
- Y. Liu, R. Hu, D. Zhang, J. Liu, F. Liu, J. Cui, Z. Lin, J. Wu, and M. Zhu, "Constructing Li-rich artificial SEI layer in alloy-polymer composite electrolyte to achieve high ionic conductivity for all-solid-state lithium metal batteries." Adv. Mater., 33, 2004711 (2021).
- Y. Liu, D. Lin, P. Y. Yuen, K. Liu, J. Xie, R. H. Dauskardt, and Y. Cui, "An artificial solid electrolyte interphase with high Li-ion conductivity, mechanical strength, and flexibility for stable lithium metal anodes." *Adv. Mater.*, 29, 1605531 (2017)
- S. Liu et al., "High interfacial-energy interphase promoting safe lithium metal batteries." J. Am. Chem. Soc., 142, 2438 (2020).
- Y. Chen et al., "Origin of dendrite-free Li deposition in concentrated electrolytes." Nat. Commun., 14, 2655 (2023).
- N.-W. Li, Y. Shi, Y.-X. Yin, X.-X. Zeng, J.-Y. Li, C.-J. Li, L.-J. Wan, R. Wen, and Y.-G. Guo, "A flexible solid electrolyte interphase layer for long-life Li metal anodes." Angew. Chem. Int. Ed., 57, 1505 (2018).
- Y. Gao and B. Zhang, "Probing the mechanically stable solid electrolyte interphase and the implications in design strategies." *Adv. Mater.*, 35, 2205421 (2023).
- Y. Xu et al., "Promoting mechanistic understanding of lithium deposition and solidelectrolyte interphase SEI formation using advanced characterization and simulation methods: recent progress, limitations, and future perspectives." Adv. Energy Mater., 12, 2200398 (2022).
- P. Arora, M. Doyle, and R. E. White, "Mathematical modeling of the lithium deposition overcharge reaction in lithium-ion batteries using carbon-based negative electrodes." *J. Electrochem. Soc.*, 146, 3543 (1999).
- X.-G. Yang, Y. Leng, G. Zhang, S. Ge, and C.-Y. Wang, "Modeling of lithium plating induced aging of lithium-ion batteries: Transition from linear to nonlinear aging." *Journal of Power Sources*, 360, 28 (2017).
- S. Hein, T. Danner, and A. Latz, "An electrochemical model of lithium plating and stripping in lithium ion batteries." ACS Appl. Energy Mater., 3, 8519 (2020).
- X. Yang, W. Li, K. Um, and D. M. Tartakovsky, "Non-equilibrium thermal models of lithium batteries." *Journal of Power Sources*, 623, 235428 (2024).
- W. Li and D. M. Tartakovsky, "Effective representation of active material and carbon binder in porous electrodes." J. Electrochem. Soc., 169, 040556 (2022).
- F. Boso, W. Li, K. Um, and D. M. Tartakovsky, "Impact of carbon binder domain on the performance of Li-metal batteries." J. Electrochem. Soc., 169, 100550 (2022).
- W. Li, "Onset of lithium plating in fast-charging li-ion batteries." ACS Energy Lett., 10, 1596 (2025).
- W. Li and D. M. Tartakovsky, "Effective models of heat conduction in composite electrodes." J. Electrochem. Soc., 170, 100503 (2023).
- C.-H. Chen and C.-W. Pao, "Phase-field study of dendritic morphology in Li metal batteries." *Journal of Power Sources*, 484, 229203 (2021).
- T. Melsheimer, M. Morey, A. Cannon, and E. Ryan, "Modeling the effects of pulse plating on dendrite growth in lithium metal batteries." *Electrochimica Acta*, 433, 141227 (2022).
- J. Wagner-Henke, D. Kuai, M. Gerasimov, F. Röder, P. B. Balbuena, and U. Krewer, "Knowledge-driven design of solid-electrolyte interphases on lithium metal via multiscale modelling," *Nat. Commun.*, 14, 6823 (2023).
- A. Cipolla, C. Barchasz, B. Mathieu, B. Chavillon, and S. Martinet, "Effect of electrochemical and mechanical properties of SEI on dendritic growth during lithium deposition on lithium metal electrode." *Journal of Power Sources*, 545, 231898 (2022).
- W. Li, H. A. Tchelepi, and D. M. Tartakovsky, "Screening of electrolyte-anode buffers to suppress lithium dendrite growth in all-solid-state batteries." *J. Electrochem. Soc.*, 170, 050510 (2023).
- C. P. Nielsen and H. Bruus, "Morphological instability during steady electrodeposition at overlimiting currents." *Phys. Rev. E*, 92, 052310 (2015).
- T. Hou, G. Yang, N. N. Rajput, J. Self, S.-W. Park, J. Nanda, and K. A. Persson, "The influence of FEC on the solvation structure and reduction reaction of LiPF<sub>6</sub>/EC electrolytes and its implication for solid electrolyte interphase formation." *Nano Energy*, 64, 103881 (2019).
- J. R. Rumble, CRC Handbook of Chemistry and Physics 104th ed. (CRC Press) (2023), Internet version.
- R. Naejus, D. Lemordant, R. Coudert, and P. Willmann, "Excess thermodynamic properties of binary mixtures containing linear or cyclic carbonates as solvents at the temperatures 298.15 K and 315.15 K." The Journal of Chemical Thermodynamics, 29, 1503 (1997).
- "CODATA value: vacuum electric permittivity." https://physics.nist.gov/cgi-bin/ cuu/Value?ep0 Accessed: 2023-07-03.
- S. Xu, K.-H. Chen, N. P. Dasgupta, J. B. Siegel, and A. G. Stefanopoulou, "Evolution of dead lithium growth in lithium metal batteries: Experimentally validated model of the apparent capacity loss." *J. Electrochem. Soc.*, 166, A3456 (2019)
- L.-G. Sundström and F. H. Bark, "On morphological instability during electrodeposition with a stagnant binary electrolyte." *Electrochimica Acta*, 40, 599 (1995).